Carbon quantum dots from pomelo peel as fluorescence probes for “turn-off–on” high-sensitivity detection of Fe 3+ and L-cysteine

Dianwei Zhang
Beijing Technology and Business University
Furui Zhang
Beijing Technology and Business University
Yonghong Liao
Beijing Technology and Business University
Fenghuan Wang
Beijing Technology and Business University
Huilin Liu (liuhuilin@btbu.edu.cn)
Beijing Technology and Business University

Research Article

Keywords: Carbon quantum dots, Turn-off–on, Pomelo peel, Fluorescence probe, Fe3+, L-Cysteine

Posted Date: March 22nd, 2022

DOI: https://doi.org/10.21203/rs.3.rs-1457300/v1

Abstract

This study designed a “turn-off–on” fluorescence analysis method based on carbon quantum dots (CQDs) to detect metal ions and amino acids in real sample systems. CQDs were derived from green pomelo peel via a one-step hydrothermal process. The co-doped CQDs with N, S atoms imparted excellent optical properties (quantum yield = 17.31%). The prepared CQDs could be used as fluorescent “turn-off” probes to detect Fe^{3+} with a limit of detection of 0.086 μM, a linear detection range of 0.1-160 μM, and recovery of 92.09%–104.87% in water samples. The quenched CQDs fluorescence could be turned on after adding L-cysteine (L-Cys), which allowed detection of L-Cys with a detection limit of 0.34 μM and linear range of 0.4–85 μM. Recovery of L-Cys in amino acid beverage was 92.58%–106.76%. Visual paper-based testing strips and cellulose/CQDs composite hydrogels could be also used to detect Fe^{3+} and L-Cys.

Introduction

Since their initial discovery in 2004, carbon quantum dots (CQDs) have drawn great attention and been widely used as novel carbon-based nanomaterials. Typically, most CQDs are spherical nanoparticles, the average diameter is usually less than 10nm (Xu et al. 2004). In the past 10 years, CQDs have attracted great attention because their superior properties of low toxicity, good biocompatibility and light resistance, easy surface modification, and environmental friendliness (Lim et al. 2015), provide good potential for use in applications such as drug delivery, sensing, biological imaging, fluorescent inks, catalysis, and light emitting diodes (Sun et al. 2016; Wang et al. 2017; Zhu et al. 2021). The obvious advantages of green chemistry have stimulated the great potential of CQDs in synthesis and application, making them an indispensable part of carbon nanomaterials. To date, many CQDs have been synthesized from biomass, such as candle root, *Prunus avium* fruit, and garlic (Hutton et al. 2016; Kumar et al. 2012; Zhao et al. 2015){Shaojing, 2015 #28}{Shaojing, 2015 #28}{Shaojing, 2015 #28}{Shaojing, 2015 #28}. Recently, heteroatom-doped CQDs have gradually emerged into the field of carbon-based nanomaterials because they can effectively adjust the composition of surface groups and change optical properties (Wang et al. 2018; Yuan et al. 2020). However, the quantum yield (QY) of one or two heteroatom-doped CQDs from biomass materials is very low, which complicates the practical application of CQDs. Therefore, there remains an urgent need for methods of large-scale preparation of high-QY biomass CQDs.

Currently, CQDs with optosensing capabilities are attracting widespread attention from researchers. In consideration of the fluorescence intensity changes of CQDs during the analysis and detection process, CQDs have been used as sensitive analytical fluorescent nanoprobes to detect certain metal ions (Cu^{2+}, Ag^{+}, Fe^{3+}, Hg^{2+}) and amino acids (Huang et al. 2018; Yan et al. 2016; Zong et al. 2014; Zou et al. 2017). Such applications are important because low levels of some heavy metal ions may cause serious physiological problems in the human body (Lars 2003). In particular, Fe^{3+} is abundant in the human body as an essential element. L-Cysteine (L-Cys) is a common and significant amino acid in living organisms

and the only one among more than 20 common amino acids that contains a thiol moiety. Because of its important physiological functions, it has promising application prospects in the biopharmaceuticals, food industry, animal feed and cosmetic industry (Liu et al. 2015; Zhou and Yoon 2012). The traditional detection methods of Fe^{3+} and L-Cys were mainly large-scale instrument chromatographic analysis methods (Mashhadizadeh et al. 2008; Matusch et al. 2010; Zhang et al. 2014). However, in general, these methods have several limitations of time-consuming pretreatments, complex operations, complicated detection processes, and relatively expensive instruments. Thus, there remains a need for a facile, rapid, inexpensive, highly sensitive and selective analytical method for simultaneous analysis of Fe^{3+} and L-Cys. Recently, Huang et al. prepared red-emitting CQDs co-doped with nitrogen–boron–sulfur to detect Ag^{+} and L-Cys in living cells and complex biological fluids (Huang et al. 2018). Yan et al. constructed a simple sensing system based on fluorescence switching of CQDs for Hg^{2+} and L-Cys analysis (Yan et al. 2016). Zong and co-workers developed an “off–on” fluorescent CQDs probe to detect Cu^{2+} and L-Cys in aqueous solution (Zong et al. 2016). Recently, Sun’s group achieved a sensitive “on–off–on” model for Hg^{2+} and L-Cys detection using nitrogen–sulfur (N-S) co-doped CQDs prepared from gardenia fruit (Sun et al. 2020). However, the low toxicity and high QY of CQDs is still a problem that we urgently need to improvement.

Herein, we describe the innovative design of CQDs with a specific and sensitive fluorescence “turn-off–on” mode, which could be used for sensitive and simple determination of Fe^{3+} and L-Cys. N-S co-doped CQDs were prepared via a one-step hydrothermal method using waste green pomelo peel as precursor. The prepared N-S co-doped CQDs could be used as efficient fluorescent “turn-off” probes for Fe^{3+} detection with high selectivity, low LOD and wide linear detection range. Interestingly, the quenched fluorescence could be “turned-on” after adding L-Cys, which could provide a high selectivity and sensitivity detection method for L-Cys in real samples. In addition, visual paper-based testing stripes and cellulose/CQDs composite hydrogels with N-S co-doped CQDs had also been used for Fe^{3+} and L-Cys detection in the solid state according to the change of color and off–on fluorescence.

Materials And Methods

Materials

Green pomelo, navel orange, and tangerine were purchased from a fruit shop in Beijing, China. $CoCl_2$, $Ba(NO_3)_2$, AgCl, $MgCl_2$, $CuSO_4$, NaCl, $CaCl_2$, $ZnCl_2$, $CdCl_2$, $NiCl_2$, and $FeSO_4{\cdot}6H_2O$ were acquired from Tianjin Chemical Reagent (Tianjin, China). $MnCl_2$, $FeCl_3{\cdot}6H_2O$, and $AlCl_3{\cdot}6H_2O$ were obtained from Aladdin. The 15 amino acids used in the study were obtained from Alfa Aesar (Tianjin) Chemical. 1-Allyl-3-methylimidazolium chloride (AmimCl) ionic liquid was acquired from Sigma-Aldrich. Dialysis bags (1000 Da molecular weight cutoff, MWCO) were supplied by MYM Biological Technology. All reagents and chemicals used in the experiments were of analytical grade and not further purified. Tap water sample was obtained from our laboratory.

Instruments

All fluorescence spectra were obtained by Synergy H1 full-function microplate reader (BioTek, USA). Transmission electron microscopy (TEM, FEI, USA) images were obtained using a Talos F200X electron microscope. Fourier transform infrared (FTIR, Nicolet Instruments, USA) spectra (400–4000 cm^{-1}) were obtained on IS10 spectrometer. X-Ray photoelectron spectroscopy (XPS, Thermo Fisher Scientific, USA) was carried out by ESCALAB 250Xi spectrometer. Fluorescence lifetime was recorded via FLS1000 fluorescence spectrometer (Edinburgh Instruments, UK). X-ray diffraction (XRD, Bruker, Germany) analysis using a D8 ADVANCE instrument using Cu Kα (λ = 0.15405 nm).

Synthesis of CQDs

The CQDs were derived via one-step hydrothermal method using waste green pomelo peel as the carbon source. Dried green pomelo peel was ground into powder in the mortar and 0.5 g of powder was dispersed in deionized water of 50 mL. Transfer the mixture to the polytetrafluoroethylene-lined stainless steel autoclave of 100 mL. After heating for 5 hours at 180 °C, then cool to ambient temperature naturally and the suspension was centrifuged at 10000 rpm for 10 min to obtain a yellow-brown supernatant. It was then filtered through a 0.22 um cellulose filter membrane and dialyzed for 24 hours using deionized water (MWCO: 1000 Da), deionized water was changed every 8 hours. Subsequently, the CQDs were obtained by evaporation of the solvent and placed in the vacuum drying oven for further drying.

For comparison, navel orange peel and tangerine peel were selected as alternative raw materials to synthesize CQDs. The same experimental steps were repeated, and the corresponding tests of fluorescence intensity were performed.

QY of CQDs

The QY of the obtained CQDs were determined by comparison method with a reference substance of quinine sulfate (QY = 56% in 0.1 M H_2SO_4) (Jiang et al. 2021). The QY_{CQDs} was calculated according to equation (1):

$$QY_{CQDs} = QY_R \times (F_{CQDS}/F_R)(A_R/A_{CQDs})(\eta_R/\eta_{CQDs}) \quad (1)$$

where F represents the integral of the fluorescence intensity,A is the absorbance at the excitation wavelength, η represents the refractive index of the solvent(1.33 for water), and subscripts R represents the reference substance quinine sulfate.

Fluorescence stability of CQDs

To evaluate fluorescence stability of the CQDs in different solvents, the CQDs were dispersed in deionized water, ethanol, acetic acid, and PBS buffer, respectively. Add aliquots of these solutions (200 μL) to 96-well plates to measure the fluorescence intensity. For a continuous investigation of fluorescence stability,

the fluorescence intensitiy of CQDs was measured every 3 days for 30 days at ambient temperature. The effect of different irradiation time (5, 10, 20, 30, 40, 50, 60, 70, 80, 90 min) with ultraviolet (UV) light was performed in a UV light box at 356 nm. The effect of different pH values on fluorescence intensity was investigated from 3 to 10. Aliquots (100 μL) NaCl solutions of different concentrations (10, 20, 50, 100, 150, 200, 300, 400, 500 mM) were added into 100 μL of CQD solution, respectively, and the fluorescence intensities were recorded.

Selectivity and interference measurements of CQDs

In the selectivity experiment, 100 μL of CQDs (0.01 $mg{\cdot}mL^{-1}$) solution was added to the 96-well plate. Aliquots of individual metal ion solution (Mg^{2+}, Ag^{+}, Zn^{2+}, Cd^{2+}, Co^{2+}, Na^{+}, Al^{3+}, Fe^{2+}, Fe^{3+}, Cu^{2+}, Ni^{2+}, Ca^{2+} , Mn^{2+}, and Ba^{2+}, 100 μL, 1 mM) were respectively mixed with CQDs solution, then the fluorescence intensity was measured, add 100 μL of Fe^{3+} solution to the CQDs solution, and measured the fluorescence intensity again. The interference of metal ions on Fe^{3+} detection by CQDs was determined by the relative fluorescence intensities of CQDs solution containing different metal ions before and after adding Fe^{3+} solution.

Sensitive detection of Fe^{3+} and L-Cys

In the Fe^{3+}detection experiment, 100 μL of Fe^{3+} solutions of different concentrations (0.1–160 μM) were added into aqueous CQDs (100 μL, 0.01 $mg{\cdot}mL^{-1}$) solutions, then 100 μL aliquots of different metal ions (1 mM) were added into the CQDs solutions for comparison. Furthermore, the states of the CQDs in Fe^{3+} solutions with different concentrations were recorded under sunlight and UV light.

Added 100 μL of L-Cys solutions (0.4–1 mM) to the mixed solutions of CQDs (100 μL, 0.01 $mg{\cdot}mL^{-1}$) and Fe^{3+} (100 μL, 4×10^{-4} $mol{\cdot}L^{-1}$) for L-Cys detection. After sufficent mixing, recorded the fluorescence intensities immediately (equilibration time 10 s). The fluorescence intensities of all samples in the experiment were recorded in the wavelength range of 360–700 nm, and the excitation wavelength was 330 nm. The optical behavior of the CQDs in the presence of the mixture was recorded under sunlight and UV light.

Tests were also performed with other amino acids in the mixture of CQDs and Fe^{3+} under the same conditions. Measurements of sensitivity and selectivity were repeated three times.

Fe^{3+} and L-Cys detection in real samples

Fe^{3+} was dissolved into the tap water to give different concentrations of 50, 100, and 400 μM for detection (excitation at 360 nm). For L-Cys detection, the amino acid beverage sample was diluted 100 times, and then mixed with CQDs solution containing Fe^{3+}. Aliquots (200 μL) of 10, 30, and 60 μM mixtures of amino acid beverage sample were added into 96-well plates for detection (excitation at 360 nm). **Preparation of cellulose/CQDs composite hydrogels**

The Cotton pulp (2.5 g) was mixed into 100 g of AmimCl and stirred vigorously rapidly at 80 °C to obtain a homogeneous solution, then placed in a vacuum oven for 4 hours to remove air bubbles. The solution was then poured slowly into 12-well plate, which was subsequently put into an AmimCl/H_2O (v/v = 1/1) coagulation bath for 24 hours. Completely remove AmimCl ionic liquid by ethanol/H_2O (v/v=1/1). The prepared cellulose hydrogels were soked in CQDs aqueous solution for 24 hours to obtain CQDs composite hydrogels.

Preparation of CQDs-based test papers

The aqueous solution of CQDs was brushed onto strip-type filter papers, which were previously treated with dimethylformamide to remove the luminescent substances. The fluorescein-free filter paper was soaked overnight in the CQDs aqueous solution. The solvent was evaporated thoroughly to obtain the CQDs-based test papers. Fe^{3+} solution and L-Cys were dripped onto the filter papers and the digital photo of the test papers was acquired in a UV light box (365 nm).

Results And Discussion

Optimization of the preparation conditions of CQDs

The detection pathway for Fe^{3+} and L-Cys based on CQDs fluorescent switch is shown in Fig. 1. Carbon sources play a very significant role in the preparation of the CQDs and there are many carbon sources for the preparation of CQDs. So far, CQDs synthesized from different carbon sources have been reported. Taking into account low toxicity of CQDs and the cost of source, biomass and its derivatives have attracted extensive attention because of their outstanding performance in availability, reproducibility and low cost. Navel orange peel, orange peel, and pomelo peel from the citrus genus of Rutaceae were used as the carbon sources for the CQDs preparation in the study (Fig.S1A-C). It was interesting that CQDs derived from pomelo peel had better fluorescence intensity than navel orange peel and orange peel (Fig. S1D). In addition, the effects of different solvents on CQDs fluorescence intensities were conducted to explore by H_2O, C_2H_6O, CH_3COOH, and phosphate buffer solution (PBS). It is obvious from Fig. S2A, the CQDs have the highest fluorescence response in aqueous solution. Then the optimum concentration of CQDs in aqueous solution was optimized (Fig. S2B). The CQDs aqueous solution (0.01 mg mL^{-1}) obtained under the optimized conditions was used for further study.

Characterization

Fig. 2A showed the particle sizes and shapes of CQDs which were obtained by TEM analysis. The TEM images showed that the prepared CQDs were uniformly distributed and could be well dispersed in aqueous solutions without apparent aggregation. High-resolution TEM images further exhibited the CQDs with a graphitic structure of clear lattice fringes about 0.21 nm. Fig. 2B showed that the synthesized CQDs were not very uniform in shape with a size range of about 1.2-8.4 nm. The average particle size of CQDs was about 5.5 nm based on 100 random nanoparticles. Typical XRD patterns of CQDs (Fig. 2D)

displayed highly disordered carbon structure with a center of broad diffraction peak at 22.1° (Tian et al. 2017).

The functional group information of CQDs was obtained through FTIR spectroscopy (Fig. 2C). The strong bands at 3442 and 2924 cm^{-1} correspond to the N-H and -CH_2 group characteristic vibrational bands on the surface of CQDs, respectively (Yuan et al. 2017; Ensafi et al. 2017). The peak at 1520-1720 cm^{-1} were attributed to C=O groups stretching vibration (Yu et al. 2015). An obvious brand at 1403 cm^{-1} was derived from the COO^- stretching vibration (Yang et al. 2017). The brand at 1260 cm^{-1} was attributed to C-N groups (Zhang et al. 2015). A stretching vibration peak at 1078 cm^{-1} was resulted from $-SO_4^{2-}$ bands (Sun et al. 2016). All these absorption peaks indicated that N and S were successful doping on the CQDs surface.

The elemental composition of CQDs was determined by XPS (Fig. 2E). There were four obvious peaks of 532.5, 399.9, 284.9, and 186.5 eV on the XPS spectrum, representing the presence of O_{1s}, N_{1s}, C_1s, and S_{2p} on the CQDs surface. According to the XPS data, the elemental composition of the CQDs was 67.96% C, 4.03% N, 27.81% O, and 0.2% S. As shown in Fig. 2F, four peaks at 288, 286.5, 286.1, and 284.7 eV in the high-resolution C_{1s} spectrum, represented O=C-O, C-O/C-N, C-S, and C-C/C=C bonds, respectively (Li et al. 2015; Lan et al. 2015). As shown in Fig. 2G, three peaks appeared at 400.5, 399.8, and 399 eV on the N_{1s} spectrum, implying the pyrrolic N, C-NH_2, and NH_3, respectively (Jiao et al. 2019). There were two main components at 165.4 and 168 eV on the S_{2p} spectrum (Fig. 2H), exhibiting that S had on the CQDs surface. The deconvolution peaks at 165.4 eV was attributed to -C-S-O bond, other components at 168 eV are attributed to -SO_4 bond (Wang et al. 2016). The XPS and FTIR spectra features confirmed that N and S were successful co-doped in the CQDs, and some relevant functional groups were existed on the CQDs surface such as amino, carboxyl, carbonyl and hydroxyl groups.

Optical properties of CQDs

The UV absorption and fluorescence spectrometry of the CQDs were investigated. As shown in Supporting Information Fig. S3A, the UV spectrum contained two typical peaks at 282 nm and 317 nm. The former was attributed to the n–π* electronic transition of the C=O bands of carboxyl groups on the surface of CQDs, while the latter was assigned to modification of other components on the CQDs surface (Ju et al. 2014; Venkateswarlu et al. 2018). The fluorescence excitation and emission spectra of CQDs aqueous solution were showed in blue and red line in Fig.S3A. The optimal emission wavelength of the CQDs was about 410 nm under the excitation wavelength about 310-350 nm. The CQDs aqueous solution was brown under natural light while it exhibited a bright blue fluorescence under the excitation of a UV light at 365 nm (Inserted Fig. S3A). Accordingly, the excitation wavelength of CQDs was further optimized in Fig. S3B. The emission wavelength showed no evident shift at 410 nm when the excitation wavelength of CQDs was set in the range of 300 nm to 360 nm. The fluorescence intensity gradually enhanced and then decreased rapidly, and the inflection point with the greatest fluorescence intensity occurred at 330 nm. Therefore, we chose 330 nm as the maximum excitation wavelength (Fig. S3B).

The optical stability of the prepared CQDs was further evaluated at ambient temperature and under UV light to evaluate the potential practical application. The preliminary experimental results showed that the CQDs had good fluorescence stability after storage at ambient temperature for 30 days (Fig. S4A). In addition, the prepared CQDs had good resistance to photobleaching, the fluorescence intensity of CQDs was almost unaffected after 90 min of continuous irradiation at 365 nm (Fig. S4B). The CQDs also maintained constant fluorescence intensity over a broad pH range increasing from 3 to 10 (Fig. S4C). The salt tolerance of CQDs was also investigated, in ultrahigh concentration NaCl (up to 1.0 M) solution, the CQDs still had strong fluorescence intensity, indicating that CQDs with the advantage of salt tolerance (Fig. S4D). The absolute QY of the CQDs reached 17.31% (Table S1). Therefore, the prepared CQDs still had good stability under extremely harsh conditions, which was beneficial to the potential applications in sensing and analysis.

Selectivity and Sensitivity

There were fifteen common metal ions used in the interference experiments to evaluate the selectivity and sensitivity of CQDs. The fluorescence intensities of CQDs containing different metal ions were studied in Fig. 3A. In order to evaluate the specificity and feasibility of prepared CQDs for the detection of Fe^{3+}, the fluorescence responses of various potentially interfering metal ions to CQDs/Fe^{3+} system at a constant concentration were investigated(Fig. 3B). These studies showed that only Fe^{3+} could effectively decrease the fluorescence intensity of the CQDs aqueous solution. This more prominent selectivity for Fe^{3+} is possibly caused by the much stronger interaction of Fe^{3+} with the CQDs than the other 14 cations. The result was intriguing, which gave us some inspiration for Fe^{3+} detection using the “turn-off” CQDs. However, after introducing L-Cys into the CQDs/Fe^{3+} system, the fluorescence intensity was recovered. Other amino acids were also tested at the same time and it was apparent that their fluorescence recovery extent was inferior to L-Cys (Fig. 3C). Accordingly, we designed a “circular pattern” by using CQDs solutions containing 15 common metal ions (Fig. 3D). Under UV light, the white circular pattern in daylight exhibited a blue fluorescence except in the presence of Fe^{3+}. Thus, CQDs/Fe^{3+} system could be successfully applied to L-Cys analysis as a “turn-on” fluorescence probe. The changes in CQDs fluorescence intensity during the proposed sensing process as shown in Fig. 1.

Optosensing of Fe^{3+} and L-Cys

To evaluate the detection performance of the prepared CQDs, fluorescence intensity was used as the evaluation index to reflect various Fe^{3+} concentrations from 0.1 to 160 μM. Fig. 4A showed that the fluorescence response of CQDs gradually decreased when the Fe^{3+} concentration increased. In addition, in the insert Fig. 4A showed that after irradiation with UV light, the blue light of CQDs aqueous solution vanished with increasing concentration of Fe^{3+}. The linear range of Fe^{3+} detection was further investigated by the changes in fluorescence intensity of CQDs (Fig. 4B). In the range of 0.1-60 μM, an obvious linear relationship was obtained with a good correlation coefficient (R^2 = 0.994). The linear

equation was fitted as $y = 0.00267x + 1.001$. The LOD was calculated as 0.086 μM according to 3 ratio of signal-to-noise.

Notably, the fluorescence signal of CQDs was gradually recovered when L-Cys was added from the concentration of 0.4 to1000 mM (Fig. 4C). The insert of Fig. 4C showed that after irradiation with UV light, the blue light of CQDs/Fe^{3+} aqueous solutions obviously recovered by increasing the content of L-Cys. Fig. 4D showed the correlation of the relative fluorescence intensity of CQDs with the concentration of L-Cys from 0.4 to 1000 mM. The relative fluorescence intensity of N/S-CQDs showed a good linear relationship with the concentration of L-Cys between 0.4-85 μM (Fig. 4D). An appropriate correlation coefficient was obtained by R^2 of 0.990. The fitted linear equation is $y = 0.00148x + 1.0734$. The LOD for L-Cys was 0.34 μM calculated by the same method as Fe^{3+} detection.

In order to further evaluate the practicability of the “turn-off-on” assay, the CQDs was applied to the detection of Fe^{3+} in laboratory tap water and L-Cys in amino acid beverage samples. None of the two samples contains the target to be measured. The recovery was calculated as difference before and after adding standard targets of 10, 30 and 60 μM, which was 83.47%–122.74% in Table S2. The results demonstrated the feasibity of the developed CQDs probe for Fe^{3+} and L-Cys detection in complex matrix. It was showed that the feasibility, reliability and application potential of the CQDs-based optosensing for detection of targets.

The repeatability of the CQDs/Fe^{3+} system for the L-Cys detection was shown in Table S3. Six repeated measurements showed no significant differences in the study. That is to say, the established detection method has good reproducibility.

Possible mechanism of “turn–off–on” mode

The photoluminescence quenching process is complex, usually including static and dynamic quenching. In this study, CQDs displayed a “turn-off-on” mode when adding Fe^{3+} and L-Cys into CQDs aqueous solution. When Fe^{3+} was added, the fluorescence intensity of CQDs was reduced (Fig. 1), which may be due to the coordination of S-containing groups of CQDs with Fe^{3+} to form Fe^{3+}-S bonds (Lu et al. 2018). But the CQDs fluorescence recovered after adding L-Cys into the CQDs/Fe^{3+} mixture, which may be caused by stronger binding interaction between Fe^{3+} and L-Cys, meaning that Fe^{3+} can be desorbed from the CQDs surface. The fluorescence sensing process can be studied with the experiments of UV absorption spectroscopy and fluorescence lifetime measurement. As shown in Fig. 5A, the characteristic absorption peak of CQDs was obviously red-shifted from 318 nm to 328 nm in the present of Fe^{3+}, indicating that Fe^{3+} formed a complex with the CQDs. However, under the present of L-Cys, the absorption peaks of the CQDs recovered to their original positions, which confirmed the removal of Fe^{3+} on the CQDs surface. Interestingly, an average fluorescence lifetime for the aqueous CQDs solution was 1.19 ns (Fig. 5B), which was essentially the same as the lifetimes for the CQDs/Fe^{3+} system (1.22 ns) and after adding L-Cys to the system (1.20 ns). These results suggested that the fluorescence quenching

mechanism was static fluorescence quenching in these processes. Combined, these results suggested that the developed CQDs could be applied as bifunctional probes for Fe^{3+} and L-Cys recognition.

Visualization cellulose/CQDs composite hydrogels and test paper

Cellulose/CQDs composite hydrogels and CQDs-based strip-type test papers (Fig. 6) were prepared using simple blending and coating processes. The composite hydrogels and CQDs-based test papers had good biocompatibility and biodegradability because they were composed of cellulose and CQDs. After the addition of Fe^{3+} (Fig. 6), the cellulose/CQDs hydrogels and CQDs-based test papers showed color changes and drop-offs in fluorescence. Surprisingly, the cellulose/ CQDs hydrogels and CQDs-based test papers then showed obvious color recovery with the addition of L-Cys. Therefore, cellulose/CQDs hydrogels and CQDs-based test papers could act as optical sensors for Fe^{3+} and L-Cys. Compared with aqueous solutions of CQDs, the CQDs-based hydrogels and test papers were easier to operate and use, and therefore had broader application prospects. More importantly, both cellulose/CQDs hydrogels and CQDs-based test papers were environmentally friendly and disposable. All these findings suggested that the prepared CQDs had great potential for applications as bifunctional sensors for recognition of Fe^{3+} and L-Cys.

Conclusions

Food waste biomass was utilized to prepare CQDs as a simple, low-toxicity dual probe for Fe^{3+} and L-Cys detection. The CQDs were prepared from green pomelo peel via one-step hydrothermal method using green pomelo peels as precursor. After co-doped with N and S atoms, the resultant CQDs solutions showed excellent optical properties, good fluorescence stabilities, and high QYs up to 17.31%. The blue emission CQDs-based “turn-off–on” fluorescent probes with high selectivity and sensitivity were developed and employed for detection of Fe^{3+} and L-Cys. The detection limit for Fe^{3+} was 0.086 μM with a linear detection range of 0.1-160 μM, and the LOD for L-Cys was 0.34 μM with a linear detection range of 0.4-85 μM. Notably, common metal ions and amino acids did not interfere with the Fe^{3+} and L-Cys detection. These traits were attributed to the sorption of Fe^{3+} on the CQDs surface, and desorption of Fe^{3+} from the CQDs via the stronger bonding of L-Cys. Therefore, low-toxicity CQDs can be considered as promising candidates for visual optical sensing in practical sample analysis. Furthermore, cellulose/CQDs composite hydrogels and CQDs-based test papers based on CQDs also showed good responsiveness to Fe^{3+} and L-Cys. The proposed CQDs probes utilize a simple “turn-off–on” fluorescent mode, providing a high-efficiency platform for ideal analytical applications in food and environmental science.

Declarations

Funding This work was supported by the National Natural Science Foundation of China (No. 31822040), the National Key R&D Program of China (No. 2018YFC1602300), and the Supported by the Research

Foundation for Youth Scholars of Beijing Technology and Business University (QNJJ2021-11).

Conflict of interest The authors declare no competing interests.

Data Availability All the data used in the manuscript are available in the tables and figures.

Authors' contributions Dianwei Zhang：Probe synthesis, data analysis and writing – original draft & editing. Furui Zhang：Characterization, fluorescence stability, selectivity sensitivity and data analysis. Yonghong Liao：Conceptualization, supervision and data analysis. Fenghuan Wang：Fe^{3+} and L-Cys detection in real samples, preparation of cellulose/CQDs composite hydrogels and CQDs-based test papers. Huilin Liu：Manuscript review & editing and data analysis.

Ethics Approval Not applicable.

Consent to participate All authors has given their full consent to participate.

Consent for publication All authors has given their full consent for publication.

References

1. Ensafi AA, Sefat SH, Kazemifard N, Rezaei B, Moradi F (2017) A novel one-step and green synthesis of highly fluorescent carbon dots from saffron for cell imaging and sensing of prilocaine. Sens Actuator B-Chem 253: 451–460.
2. Huang S, Yang E, Yao JD, Liu Y, Xiao Q (2018) Red emission nitrogen, boron, sulfur co-doped carbon dots for “on-off-on” fluorescent mode detection of Ag^{+} ions and L-cysteine in complex biological fluids and living cells. Anal Chim Acta 1035: 192–202.
3. Hutton GAM, Reuillard B, Martindale BCM, Caputo CA, Lockwood CWJ, Butt JN, Reisner E (2016) Carbon dots as versatile photosensitizers for solar-driven catalysis with redox enzymes. J Am Chem Soc 138: 16722-16730.
4. Jiang W, Zhao Y, Zhang DW, Zhu XC, Liu HL, Sun BG (2021) Efficient and robust dual modes of fluorescence sensing and smartphone readout for the detection of pyrethroids using artificial receptors bound inside a covalent organic framework. Biosens Bioelectron 194: 113582.
5. Jiao Y, Gao YF, Meng YT, Lu WJ, Liu Y, Han H, Shuang SM, Li L, Dong C (2019) One-step synthesis of label-free ratiometric fluorescence carbon dots for the detection of silver ions and glutathione and cellular imaging applications. ACS Appl Mater Interfaces 11: 16822–16829.
6. Ju J, Zhang RZ, He SJ, Chen W (2014) Nitrogen-doped graphene quantum dots-based fluorescent probe for the sensitive turn-on detection of glutathione and its cellular imaging RSC Adv 4: 52583–52589.
7. Kumar P, Bohidar HB (2012) Physical and fluorescent characteristics of non-functionalized carbon nanoparticles from candle soot. J Nanopart Res 14: 948.

8. Lan MH, Zhang JF, Chui YS, Wang H, Yang QD, Zhu XY, Wei HX, Liu WM, Ge JC, Wang PF, Chen XF, Lee CS, Zhang WJ (2015) A recyclable carbon nanoparticle-based fluorescent probe for highly selective and sensitive detection of mercapto biomolecules. J Mater Chem B 3: 127–134.
9. Lars J (2003) Hazards of heavy metal contamination. Br Med Bull 68: 167–182.
10. Li LB, Yu B, You TY (2015) Nitrogen and sulfur co-doped carbon dots for highly selective and sensitive detection of Hg (□) ions. Biosens Bioelectron 74: 263–269.
11. Lim SY, Shen W, Gao ZQ (2015) Carbon quantum dots and their applications. Chem Soc Rev 44: 362–381.
12. Liu YW, Lv X, Hou M, Shi YW, Guo W (2015) Selective fluorescence detection of cysteine over homocysteine and glutathione based on a cysteine-triggered dual michael addition/retro-aza-aldol cascade reaction. Anal Chem 87: 11475–11483.
13. Lu MC, Duan YX, Song YH, Tan JS, Zhou L (2018) Green preparation of versatile nitrogen-doped carbon quantum dots from watermelon juice for cell imaging, detection of Fe^{3+} ions and cysteine, and optical thermometry. J Mol Liq 269: 766–774.
14. Mashhadizadeh MH, Azimi MS, Pesteh M, Sheikhshoaei I, Ardakani MM, Karimi MA (2008) Flame atomic absorption spectrometric determination of μg amounts of Fe(III) ions after solid phase extraction using modified octadecyl silica membrane disks. Spectroc Acta Pt B-Atomic Spectr 63: 889–892.
15. Matusch A, Depboylu C, Palm C, Wu B, Hoglinger GU, Schafer MKH, Becker JS (2010) Cerebral bioimaging of Cu, Fe, Zn, and Mn in the MPTP mouse model of Parkinson's disease using laser ablation inductively coupled plasma mass spectrometry (LA-ICP-MS). J Am Soc Mass Spectrom 21: 161–171.
16. Sun S, Zhang L, Jiang K, Wu A, Lin HW (2016) Toward high-efficient red emissive carbon dots: facile preparation, unique properties, and applications as multifunctional theranostic agents. Chem Mater 28: 8659–8668.
17. Sun D, Liu TT, Wang CF, Yang LF, Yang SK, Zhuo KL (2020) Hydrothermal synthesis of fluorescent carbon dots from gardenia fruit for sensitive on-off-on detection of Hg(2+) and cysteine. Spectroc Acta Pt A-Molec Biomolec Spectr 240: 118598.
18. Sun C, Zhang Y, Wang P, Yang Y, Wang Y, Xu J, Wang YD, Yu WW (2016) Synthesis of nitrogen and sulfur co-doped carbon dots from garlic for selective detection of Fe^{3+}. Nanoscale Res Lett 11: 110.
19. Tian T, He Y, Ge YL, Song GW (2017) One-pot synthesis of boron and nitrogen codoped carbon dots as the fluorescence probe for dopamine based on the redox reaction between Cr(VI) and dopamine. Sens Actuator B-Chem 240: 1265–1271.
20. Venkateswarlu S, Viswanath B, Reddy AS, Yoon MY (2018) Fungus-derived photoluminescent carbon nanodots for ultrasensitive detection of Hg^{2+} ions and photoinduced bactericidal activity. Sens Actuator B-Chem 258: 172-183.

21. Wang HY, Lu QJ, Hou YX, Liu YL, Zhang YY (2016) High fluorescence S, N co-doped carbon dots as an ultra-sensitive fluorescent probe for the determination of uric acid. Talanta 155: 62–69.
22. Wang YF, Zhu YW, Yu SM, Jiang CL (2017) Fluorescent carbon dots: rational synthesis, tunable optical properties and analytical applications. RSC Adv 7: 40973–40989.
23. Wang G, Guo QL, Chen D, Liu ZD, Zheng XH, Xu AL, Yang SW, Ding GQ (2018) Facile and highly effective synthesis of controllable lattice sulfur-doped graphene quantum dots via hydrothermal treatment of durian. ACS Appl Mater Interfaces 10: 5750–5759.
24. Xu XY, Ray R, Gu YL, Ploehn HJ, Gearheart L, Raker K, Scrivens WA (2004) Electrophoretic analysis and purification of fluorescent single-walled carbon nanotube fragments. J Am Chem Soc 126: 12736–12737.
25. Yan FY, Shi DC, Zheng TC, Yun KY, Zhou XG, Chen L (2016) Carbon dots as nanosensor for sensitive and selective detection of Hg^{2+} and L-cysteine by means of fluorescence “off-on” switching. Sens Actuator B-Chem 224: 926–935.
26. Yang R, Guo XF, Jia LH, Zhang Y, Zhao ZL, Lonshakov F (2017) Green preparation of carbon dots with mangosteen pulp for the selective detection of Fe^{3+} ions and cell imaging. Appl Surf Sci 423: 426–432.
27. Yu J, Song N, Zhang YK, Zhong SX, Wang AJ, Chen JR (2015) Green preparation of carbon dots by Jinhua bergamot for sensitive and selective fluorescent detection of Hg^{2+} and Fe^{3+}. Sens Actuator B-Chem 214: 29–35.
28. Yuan FL, Wang ZB, Li XH, Li YC, Tan ZA, Fan LZ, Yang SH (2017) Bright multicolor bandgap fluorescent carbon quantum dots for electroluminescent light-emitting diodes. Adv Mater 29: 1604436.
29. Yuan XY, Jiang W, Wang J, Liu HL, Sun BG (2020) High-performance multiporous imprinted microspheres based on N-doped carbon dots exfoliated from covalent organic framework for flonicamid optosensing. ACS Appl Mater Interfaces 12: 25150–25158.
30. Zhang HQ, Huang YH, Hu SR, Huang QT, Wei C, Zhang WX, Kang LP, Huang ZY, Hao AY (2015) Fluorescent probes for "off-on" sensitive and selective detection of mercury ions and L-cysteine based on graphitic carbon nitride nanosheets. J Mater Chem C 3: 2093–2100.
31. Zhang WB, Li PL, Geng QQ, Duan YH, Guo MC, Cao YS (2014) Simultaneous determination of glutathione, cysteine, homocysteine, and cysteinylglycine in biological fluids by ion-pairing high-performance liquid chromatography coupled with precolumn derivatization. J Agric Food Chem 62: 5845–5852.
32. Zhao SJ, Lan MH, Zhu XY, Xue HT, Ng TW, Meng XM, Lee CS, Wang PF, Zhang WJ (2015) Green synthesis of bifunctional fluorescent carbon dots from garlic for cellular imaging and free radical scavenging. ACS Appl Mater Interfaces 7: 17054–17060.
33. Zhou Y, Yoon J (2012) Recent progress in fluorescent and colorimetric chemosensors for detection of amino acids. Chem Soc Rev 41: 52–67.

34. Zhu XC, Yuan XY, Han LX, Liu HL, Sun BG (2021) A smartphone-integrated optosensing platform based on red-emission carbon dots for real-time detection of pyrethroids. Biosens Bioelectron 191: 113460.
35. Zong J, Yang XL, Trinchi A, Hardin S, Cole I, Zhu YH, Li CZ, Muster T, Wei G (2014) Carbon dots as fluorescent probes for “off-on” detection of Cu^{2+} and L-cysteine in aqueous solution. Biosens Bioelectron 51: 330–335.
36. Zou SY, Hou CJ, Fa HB, Zhang L, Ma Y, Dong L, Li D, Huo DQ, Yang M (2017) An efficient fluorescent probe for fluazinam using N, S co-doped carbon dots from L-cysteine. Sens Actuator B-Chem 239: 1033–1041.

Scheme

Scheme 1 is available in Supplementary Files section.

Figures

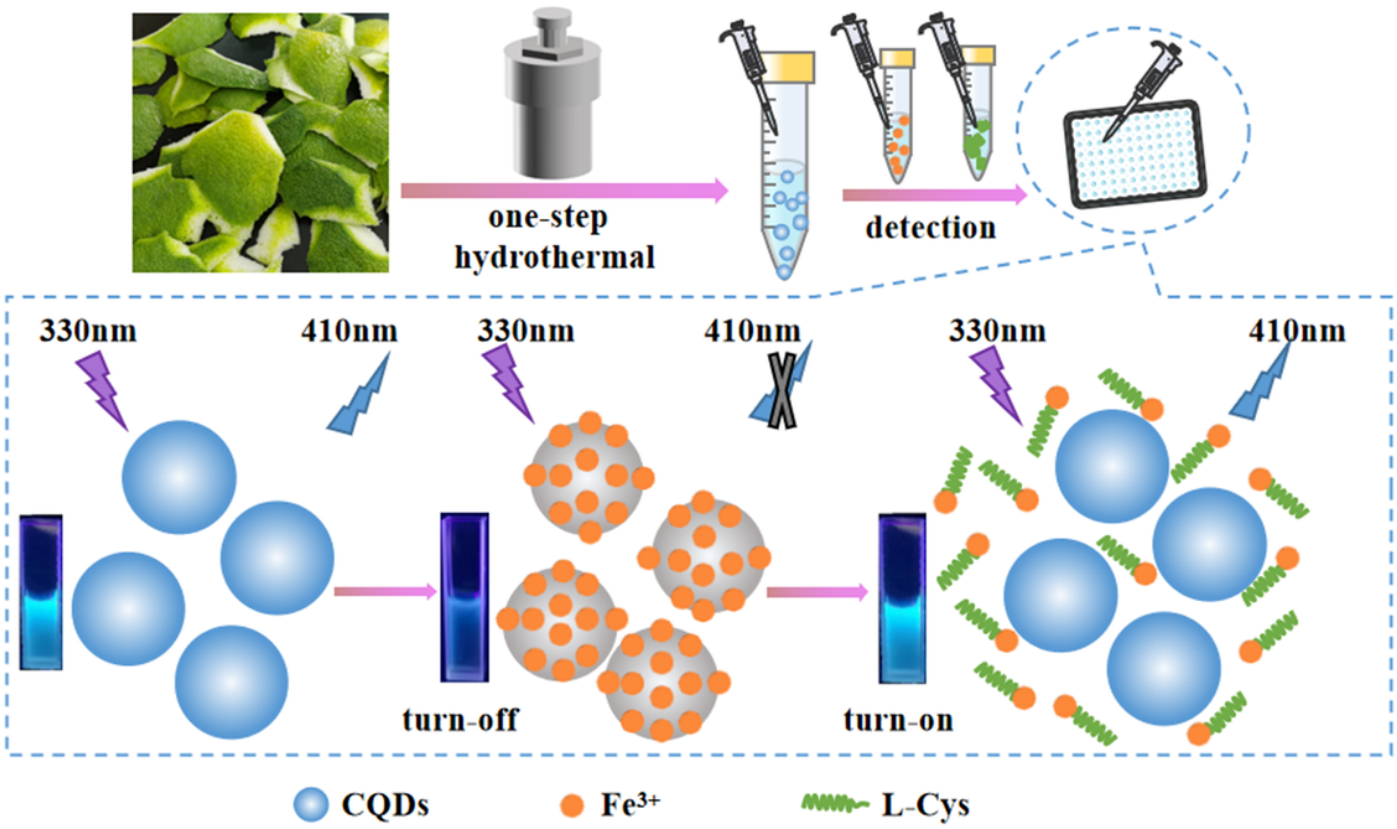

Figure 1

Schematic representation of the detection principle for Fe^{3+} and L-Cys based on CQDs.

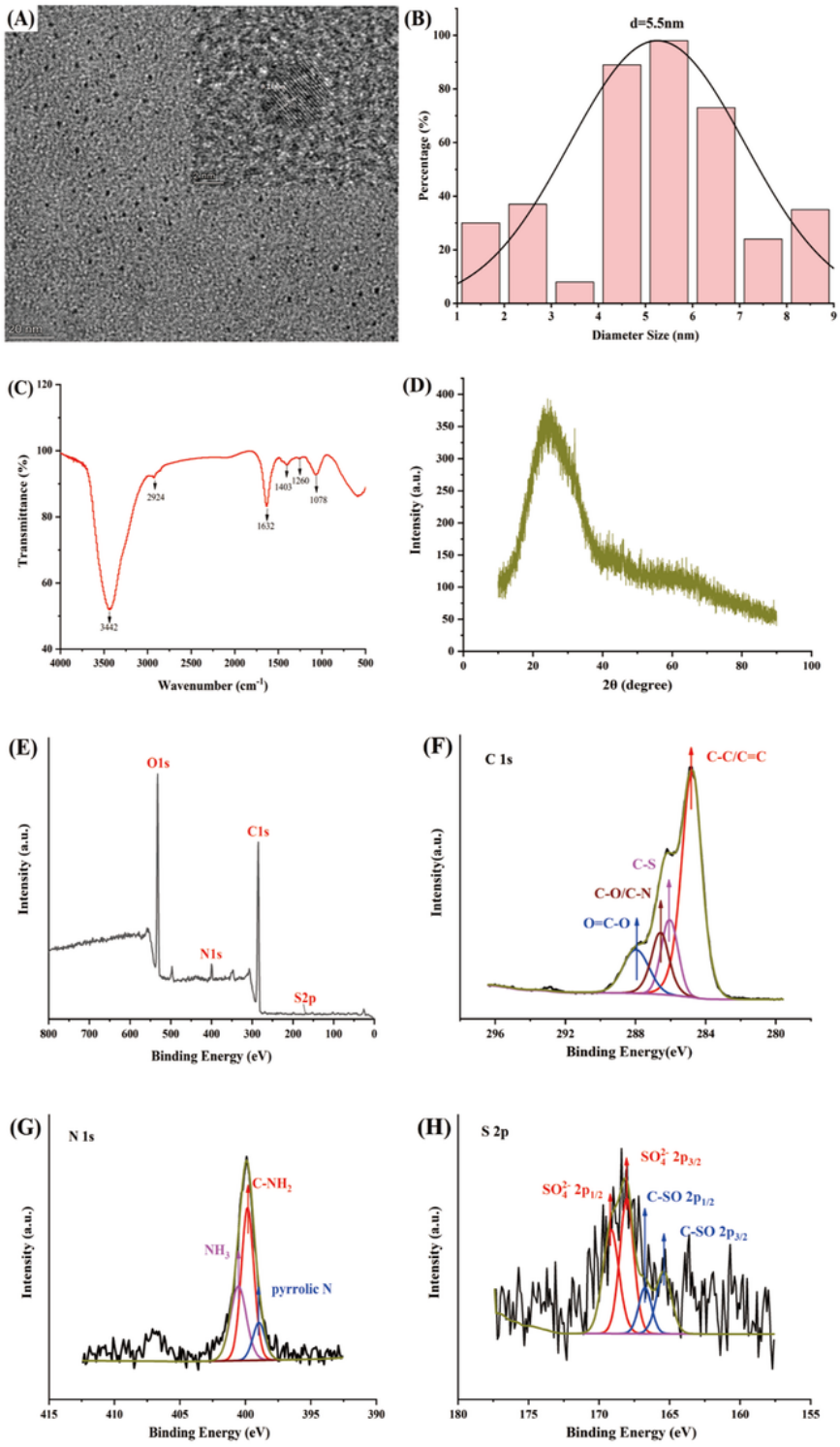

Figure 2

(A) TEM images of CQDs, Insert: High-resolution TEM images of CQDs. (B) The size distribution histogram of CQDs. (C) FT-IR of CQDs. (D) XRD of CQDs. (E) XPS of CQDs. (F-H) High-resolution spectra of C1s, N1s, and S2p for the CQDs.

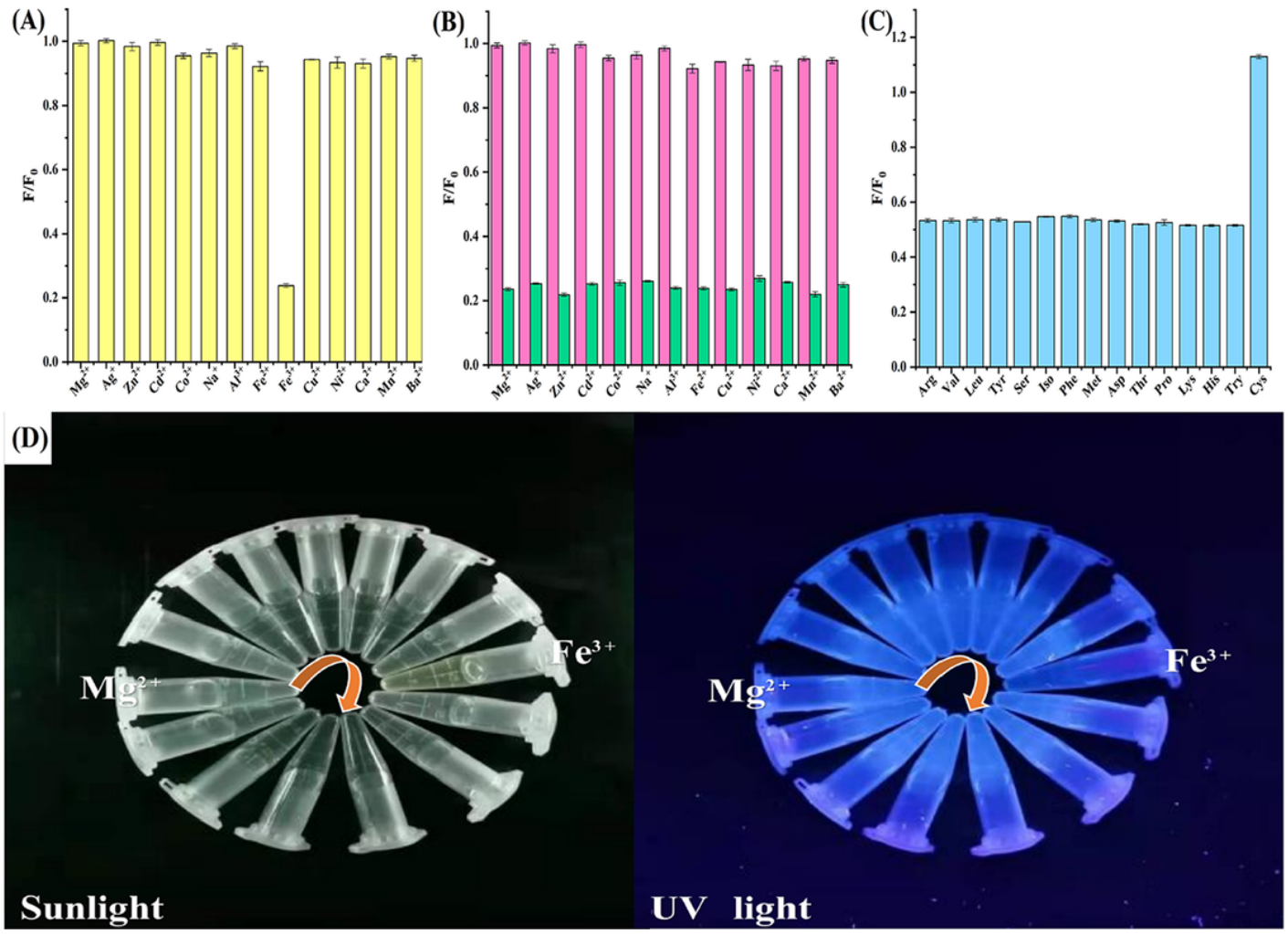

Figure 3

(A) Influences of metal ions (1 mM) on fluorescence intensity of CQDs. (B) Influences of metal ions (1 mM) on fluorescence intensity of CQDs/Fe^{3+} system. (C) Influences of amino acids (1 mM) on fluorescence intensity of CQDs/Fe^{3+}/L-Cys system. (D) Selectivity experiments under sunlight and UV light (365 nm, red arrow is consistent with the abscissa of Fig. 2A).

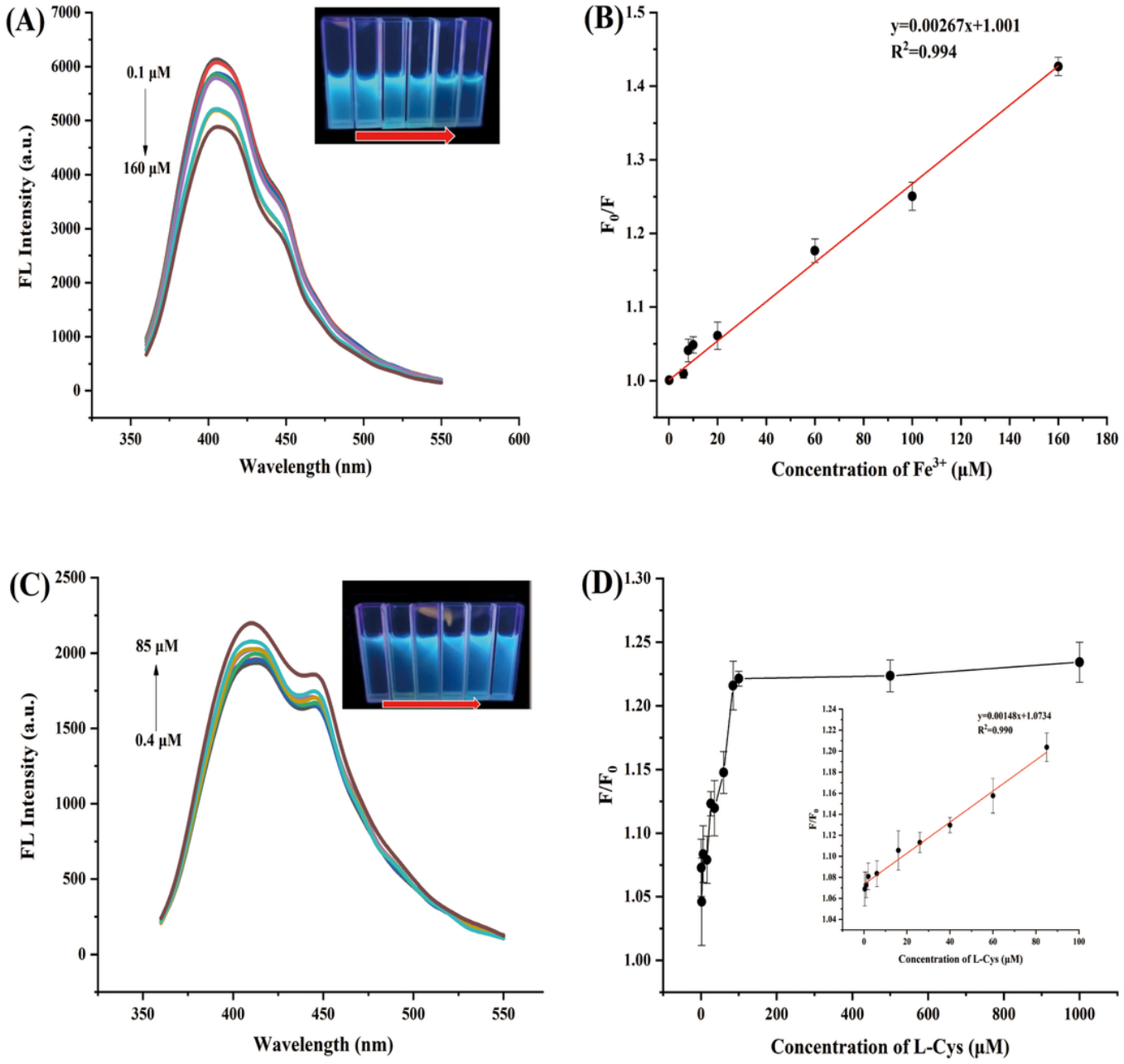

Figure 4

(A) Fluorescence spectra of CQDs (0.01 mg/mL) with various Fe^{3+} concentrations of 0.1-160 μM. Insert: photograph of CQDs with Fe^{3+} solutions under UV light (concentrations of Fe^{3+} are 0.1, 6, 10, 20, 100, and 160 μM; follow red arrow). (B) Relationship of F_0/F and Fe^{3+} concentration. (C) Fluorescence spectra of CQDs/Fe^{3+} systems of different concentrations of L-Cys. Insert: image of CQDs/Fe^{3+} aqueous solutions treated with different concentrations of L-Cys under UV light (concentrations of L-Cys are 0.4, 6, 16, 26, 40, and 85 μM; follow red arrow). (D) Relationship of F_0/F and L-Cys concentration. Insert: Linear relationship between F_0/F of CQDs and concentration of L-Cys from 0.4 μM to 85 μM.

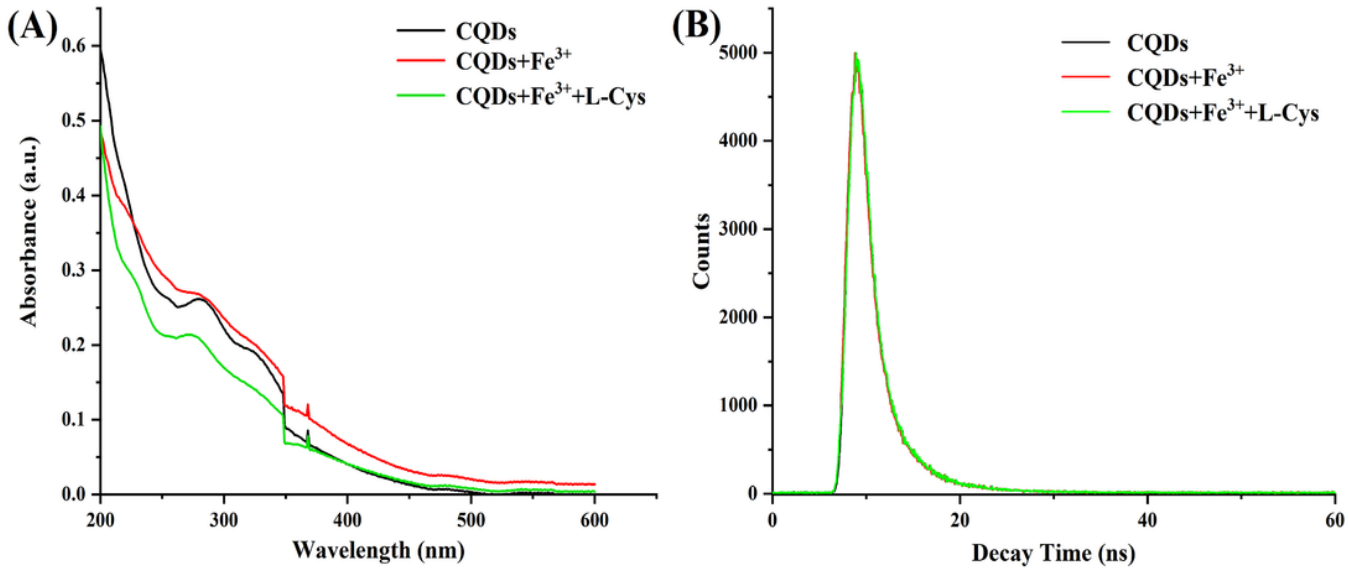

Figure 5

(A) UV–vis spectra and (B) Fluorescence spectra of CQDs, CQDs/Fe^{3+}, and CQDs/Fe^{3+}/L-Cys.

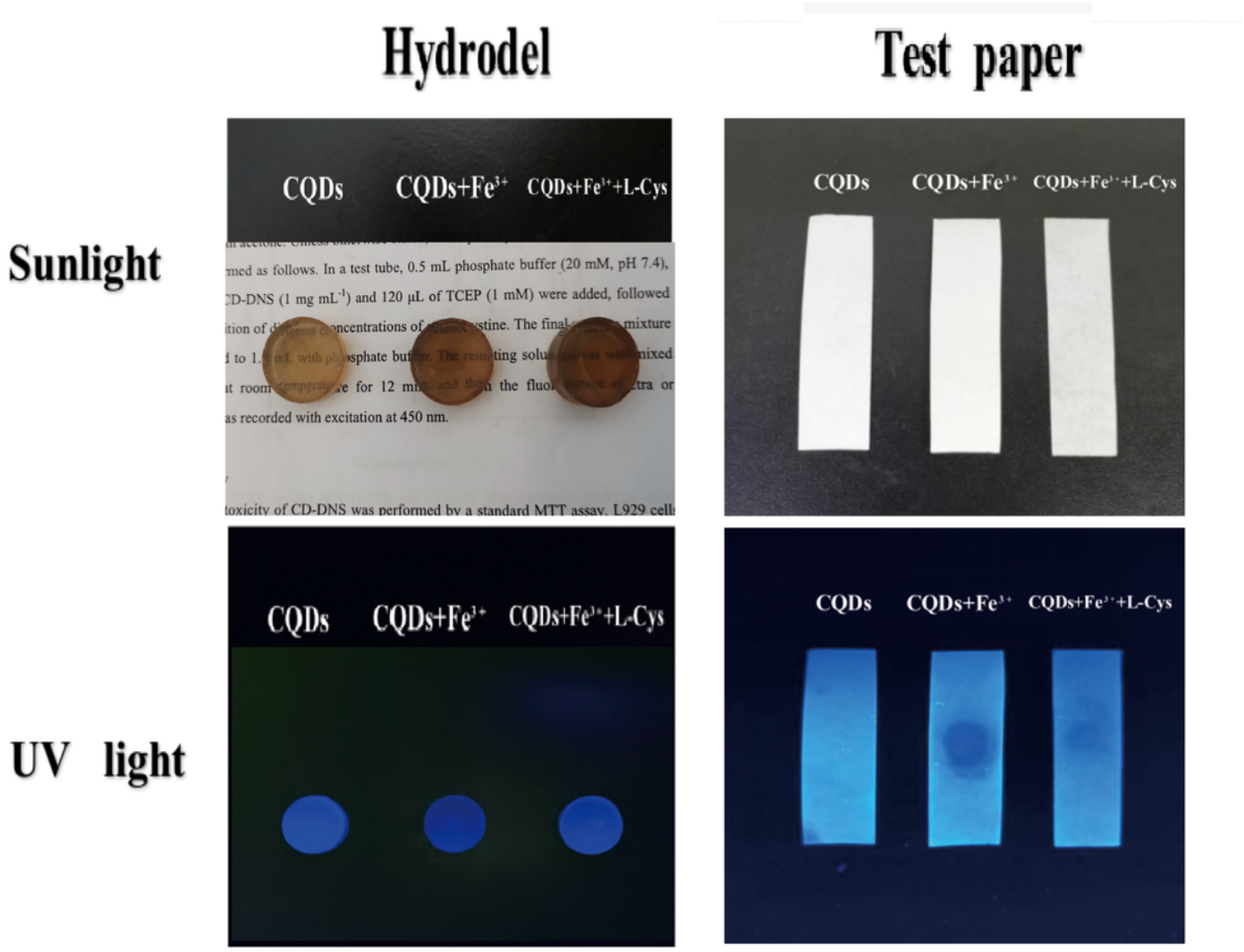

Figure 6

Photographs of the cellulose/ CQD composite hydrogels and CQDs-based test papers for the colorimetric and fluorescent detection of L-Cys under irradiation of sunlight and UV light (365 nm).

Supplementary Files

This is a list of supplementary files associated with this preprint. Click to download.

- SI.docx
- Scheme1.png